THEORY AND SIMULATIONS OF SOLAR ATMOSPHERE DYNAMICS

Robert F. Stein[1], Tom J. Bogdan[2], Mats Carlsson, Viggo Hansteen, Andrew McMurry, Colin S. Rosenthal[3], and Åke Nordlund[4]

[1]Physics & Astronomy Department, Michigan State University, East Lansing, MI 48824, USA
[2]High Altitude Observatory, NCAR, Boulder, CO 80307, USA
[3]Institute of Theoretical Astrophysics, University of Oslo, Blindern, N–0315 Oslo, Norway
[4]NBIfAFG, Københavns Universitet, København Ø, DK-2100, Denmark

ABSTRACT

Numerical simulations are used to study the generation and propagation of waves in the solar atmosphere. Solar p-mode oscillations are excited by turbulent pressure work and entropy fluctuations (non-adiabatic gas pressure work) near the solar surface. Interactions between short and long period waves and radiative energy transfer control the formation of shocks. The magnetic structure of the atmosphere induces coupling among various MHD wave modes, with intense coupling and wave transformation at the beta equal one surface, which likely is the location of the so-called "magnetic canopy".

Key words: MHD Waves; p-Modes; Shocks.

1. INTRODUCTION

Acoustic and magnetic waves and magnetic field reconnection are thought to be responsible for the heating of the solar atmosphere. Biermann (1948) and Schwarzschild (1948) first proposed that shock waves heat the solar chromosphere, while at the same time it was recognized that magnetic waves must also be present (Alfvén 1947). In a seminal paper, Osterbrock (1961) made the first thorough study of the generation, propagation, dissipation and heating of the solar atmosphere by acoustic and magnetic waves.

There is an extensive literature on wave generation by turbulence, developed to reduce jet engine noise and submarine propeller noise, and in astrophysics to explain chromospheric and coronal heating and p-mode excitation. MHD waves and P-mode oscillations are excited by turbulent convection which produces fluctuating Reynolds stresses (turbulent pressure), entropy fluctuations, and buffets and twists magnetic field lines. Wave generation by turbulent convection calculations are generally based on the work of Lighthill (1952), who separated the variables into an adiabatic linear part due to the wave motions and non-adiabatic and non-linear parts due to the turbulence and derived an inhomogeneous wave equation for one of the variables with the non-linear turbulence terms as a source. Proudman (1952) was the first to obtain quantitative estimates of the rate of sound generation by turbulent fluid motions. These calculations were extended for acoustic waves to the stratified solar atmosphere by Unno & Kato (1962), Stein (1967) and Musielak et al. (1994). Kulsrud (1955) and Lighthill (1960) extended the method to include magnetic fields. More recently, Ulmschneider and Musielak (1998, 2001) and Luo et al. (2002) have calculated the generation of magnetic waves using similar techniques. Similar approaches to wave generation were used by Balmforth (1992), Goldreich, Murray & Kumar (1994), and Samadi & Goupil (2001) to calculate p-mode oscillation excitation rates. These analytic approaches all require many approximations and a knowledge of the spectral properties of the turbulent solar convection. Now it is possible to calculate the wave generation and mode excitation numerically from realistic simulations of solar convection without the need for such simplifying assumptions or if desired to determine the actual spatial and temporal spectral properties of the convection to use in the simplified analytic excitation expressions (Skartlien, Stein & Nordlund 2000, Stein & Nordlund 2001).

Atmospheric heating and dynamics depends on wave propagation properties as well as the wave generation. The crucial issues are wave refraction, reflection, coupling between wave modes and dissipation. Osterbrock (1961) pointed out the importance of refraction with increasing Alfven speed in limiting the amount of magnetoacoustic wave energy reaching the upper chromosphere. Bazer (1961), Frisch (1964) and Stein (1971) calculated the coupling of MHD wave modes in a stratified atmosphere with curved magnetic field lines. Wave mode coupling converts acoustic fast modes generated in the convection zone into acoustic slow modes and magnetic fast and Alfven modes near the layer where the sound and Alvén speeds are equal. Fast modes propagate in all directions and are subject to refraction, but slow and Alfvén modes propagate along the magnetic field. Recently, MHD wave propagation has been studied by Musielak (1995), Ziegler and Ulmschneider (1997), Cargill, Spicer and Zalesak (1997), Tirry & Berghmans (1997), Huang,

Musielak & Ulmschneider (1999), Sakai et al. (2001), Bodo et al. (2000), Mckenzie and Axford (2000), De Groof & Goossens (2000), De Groof et al. (2002), Tsiklauri, Nakariakov & Rowlands (2003), Musielak and Ulmschneider (2003), and Arregui, Oliver and Ballester (2003).

Finally, to heat the chromosphere and corona the energy propagated to those regions must be converted from wave to thermal energy by the dissipation of the waves. For acoustic waves this occurs via shocks (see e.g. Landau & Lifschitz Fluid Mechanics). Recently Carlsson & Stein (1992, 1997) have studied the propagation of radiating acoustic shocks through the solar chromosphere and shown that they are responsible for the CaII K2V bright points and also raised questions about whether acoustic shocks are capable of heating a non-magnetic chromosphere (Carlsson & Stein 1995). Other calculations of chromospheric heating by shock dissipation have been performed by Fawzy et al. (2002), Rammacher & Cuntz (2003), Cuntz et al. (1999) and Buchholz, Ulmschneider & Cuntz (1998). Fast modes are also compressible and can shock. Alfvén waves don't shock, though they do become non-linear, and there have been many mechanisms proposed for their dissipation, for example resonant absorption (Ionson 1978, Lee and Roberts 1986, Goossens & De Groof 2001), phase mixing (Heyvaerts & Priest 1983, De Moortel, Hood & Arber 2000), and wave leakage (Cally 1986, Stenuit, Keppens & Goossens 1998) and plasma effects (Goodman 2000). We do not discuss these dissipation issues further here.

MHD wave generation, coupling and dissipation are also important in accretion disks around compact stars, the interstellar medium and plasma fusion machines.

2. WAVE EXCITATION

Waves are excited in the solar atmosphere by the PdV work of turbulent pressure (Reynolds stress) fluctuations, non-adiabatic gas pressure (entropy) and magnetic field line motions produced by convection. Both wave pulse generation and stochastic excitation of resonant modes occurs.

2.1. Impulsive Excitation

Waves are excited impulsively when there is a rapid change in the vertical velocity at the top of the convection zone (Skartlien, Stein & Nordlund 2000). When a small granule is squeezed out of existence and the upward granular velocity changes to a downflow in a time short compared to the acoustic cutoff period, then first a low pressure rarefaction is produced above the disappearing granule and the region turns dark as the transport of energy to the surface declines(Fig. 1). This is followed by horizontal inflow driven by the horizontal pressure gradient, which produces a high pressure compression above the location of the former granule and launches a compression wave into the solar atmosphere (Fig. 2). As wave propagates through the atmosphere it leaves behind a wake which oscillates up and down. The upward propagating acoustic pulse steepens into a shock in the mid-chromosphere.

2.2. Stochastic Excitation

Waves and p-mode oscillations are also excited stochastically by the PdV work of turbulent and non-adiabatic gas pressure fluctuations, Reynolds stress and entropy fluctuations respectively, produced by convection. The rate of energy input to the modes can be calculated starting with the kinetic energy equation for the modes (Nordlund & Stein (2001). Neglecting the viscous stresses,

$$\rho \frac{D}{Dt}\left(\frac{1}{2}u_z^2\right) = -\frac{\partial}{\partial z}\left[u_z\left(P_g+P_t\right)\right] + \rho u_z g + \left(P_g+P_t\right)\frac{\partial u_z}{\partial z}\,. \quad (1)$$

After integrating this equation over depth, the flux divergence term only gives contributions from the end points and is negligible. The buoyancy term is small because mass is conserved so there is no net mass flux. The last term is the PdV work,

$$W = \int dt \int dz \delta P \frac{\partial \dot{\xi}}{\partial z}\,. \quad (2)$$

There are several contributions to this work. The displacement, ξ, has contributions from the modes as well as the random convective motions. The pressure, δP, has coherent contributions from the modes and incoherent contributions from the random convective motions. Both coherent and incoherent contributions can be further divided into adiabatic and non-adiabatic terms. The dominant driving comes from the interaction of the non-adiabatic, incoherent pressure fluctuations,

$$\delta P^{\rm nad} = \left(\delta \ln P - \Gamma_1 \delta \ln \rho\right) P\,, \quad (3)$$

with the coherent mode displacement,

$$\frac{\partial \dot{\xi}}{\partial z} = -\frac{D \ln \rho}{Dt}\,. \quad (4)$$

The total pressure fluctuation is the sum of the turbulent and non-adiabatic gas pressure fluctuations,

$$\delta P = \delta P_{\rm turb} + \delta P_{\rm gas}^{\rm nad} \quad (5)$$

The turbulent pressure is

$$\delta P_{\rm turb} = \delta \left\langle \rho \delta V_z^2 \right\rangle \quad (6)$$

This is a stochastic process, so the pressure fluctuations occur with random phases with respect to the modes. Therefore one must average over all possible relative phases between them. The resulting rate of energy input to the modes is (Nordlund & Stein (2001)

$$\frac{\Delta \langle E_\omega \rangle}{\Delta t} = \frac{\omega^2 \left| \int_r dr \delta P_\omega^* \frac{\partial \xi_\omega}{\partial z} \right|^2}{8 \Delta \nu E_\omega}\,. \quad (7)$$

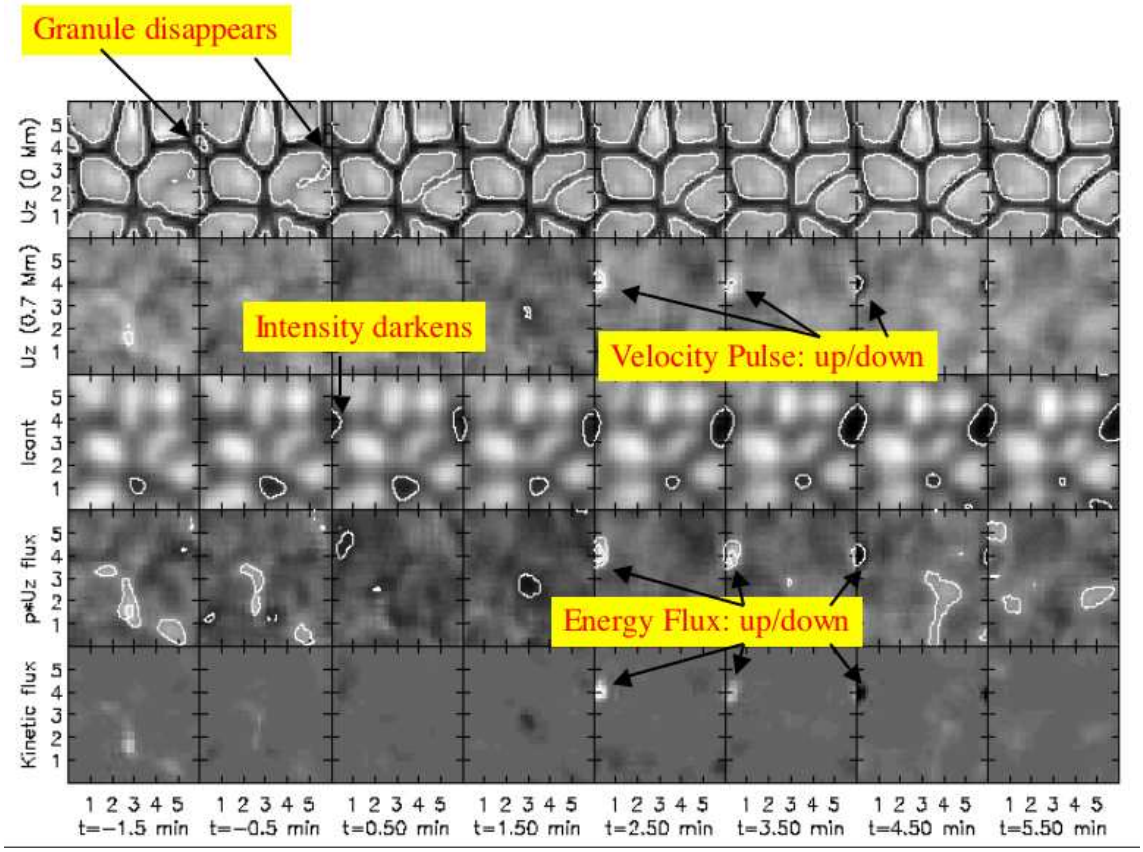

Figure 1. A time sequence of horizontal slices of from top to bottom: vertical velocity at the surface and at 700 km, continuum intensity, acoustic flux (Pu_z) and kinetic energy flux ($1/2\rho\mathbf{u}^2u_z$). The spatial tick marks are 1 Mm intervals. The production of an acoustic pulse is illustrated.

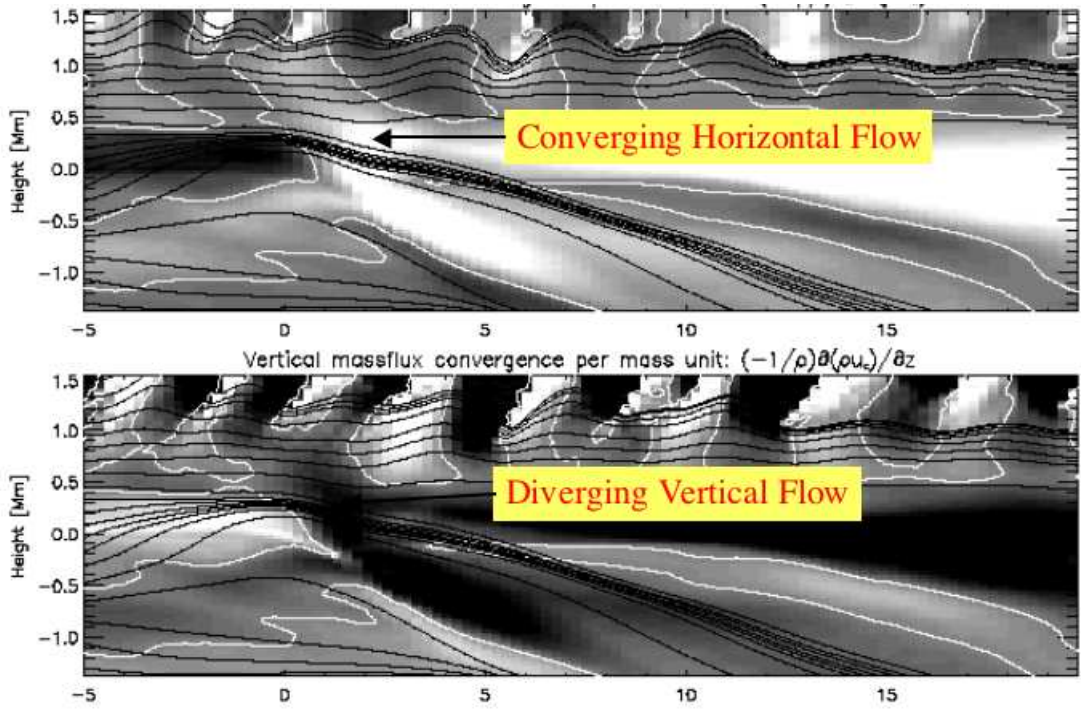

Figure 2. Time evolution of a horizontal and vertical mass flow convergence/divergence along a vertical line through the center of wave pulse source.

Here, δP_ω is the time Fourier transform of the non-adiabatic total pressure. $\Delta\nu = 1/$(total time interval) is the frequency resolution with which δP_ω is computed. ξ_ω is the mode displacement eigenfunction, which is typically chosen to be real for an adiabatic mode. In that case, taking the complex conjugate of the pressure is not necessary, but we retain it for generality. The mode energy is

$$E_\omega = \frac{1}{2}\omega^2 \int_r dr\ \rho\ \xi_\omega^2 \left(\frac{r}{R}\right)^2 = M_\omega V_\omega^2(R)\ . \quad (8)$$

Here M_ω is the mode mass and $V_\omega(R)$ is the mode velocity amplitude at the surface. Eqn 7 is similar to the expressions of Goldreich, Murray & Kumar (1994) (eqn. 26) and (Samadi & Goupil 2001), but involves no approximations. With realistic numerical simulation data (Stein & Nordlund 2000) we can evaluate this expression exactly without having to make approximations in order to evaluate it analytically.

Convection consists of slow, diverging, fairly laminar, warm upflows and fast, converging, turbulent, cool downflows (Fig. 3). Both the turbulent pressure and entropy fluctuations are largest in the cool downflows near the solar surface where the convective velocities and vorticity are largest and the energy transport switches between convective and radiative with small local, transitory imbalances (Fig. 4).

The simulated excitation rates are in good agreement with the solar observations from SOHO (Fig. 5). The excitation decreases at low frequencies because of the mode properties: the mode mass increases toward lower frequencies and mode compression decreases toward lower frequencies. The excitation decreases at high frequencies because of the convection properties: convection is a low frequency phenomenon, so the pressure and entropy fluctuations it produces are primarily at low frequencies (Stein & Nordlund 2001).

P-mode and wave excitation is a surface phenomena. The turbulent velocity and vorticity peak in the superadiabatic layer just below the surface. The largest entropy fluctuations occur at the top of the superadiabatic layer. At low frequencies the driving is smaller but more spread out. At high frequencies it is confined close to the surface. The maximum driving is within 400 km of the surface in the peak driving frequency range of 3-4 mHz (Fig. 6).

There has been considerable controversy over the existence or non-existence of high frequency ($\sim$ 30 mHz) acoustic waves to heat the solar chromosphere. Observations can not settle this issue because they can not see such short wavelength waves whose size is comparable to that of line contribution functions. Our highest resolution simulations have a grid size of 25 km. Waves with wavelengths greater than 10 grid zones (=250 km) should propagate accurately in the calculations. Such waves would have a period of about 36 sec or frequency of 30 mHz. There is no indication in the acoustic flux from our simulations that such waves carry a significant amount of energy (Fig. 7). The acoustic flux falls off rapidly at frequencies above 10 mHz.

3. HYDRODYNAMIC WAVE PROPAGATION

Acoustic waves in non-magnetic regions, acoustic fast waves in weak field regions and acoustic slow waves or longitudinal "tube" waves in strong field magnetic regions (Alfvén speed greater than sound speed) steepen and form shocks. Their wave crests travel slightly faster than the wave troughs because the crests have larger sound and fluid speeds. Thus the crests eventually overtake the troughs and a wave front with steep gradients (shock) develops. Magnetic fast mode waves in strong field regions are also compressible and steepen into shocks. Shocks convert the kinetic energy of the wave motion into heat, excitation and ionization energy.

The clearest evidence for shocks in the solar chromosphere is the behavior of the Ca II H & K bright grains. Carlsson & Stein (1997) have shown that the behavior of the Ca II H & K lines is explained by the occurrence of acoustic shocks in the mid chromosphere. They used a one-dimensional, radiation-hydrodynamic code, with non-LTE radiation transfer including 6 level model atoms for hydrogen and calcium plus background continua, on an adaptive grid which achieves a spatial resolution of 0.1 km. Acoustic waves are driven through the atmosphere by a piston below the visible surface whose velocity was chosen to match the Doppler shift observations in a photospheric iron line formed about 260 km above $\tau_{500} = 1$. These acoustic waves steepen into shocks in the mid-chromosphere and intermitantly heat the plasma there. The calculated Ca H line intensity closely matches the observed intensities (Fig. 8). There are some differences. The simulated bright grains occur at nearly the same time as the observed ones, but slightly delayed. The amplitude of the intensity variation is nearly that observed, but about 20faint in the simulations. That there is not perfect agreement is not surprising as there is still physics missing from the simulation: The simulation is one-dimensional rather than three so there are no horizontal radiative losses from the waves nor any interference of waves originating at different spatial locations at the top of the convection zone. There is no Mg II or CO line radiation in the simulation which will increase the cooling and further weaken the waves. There is complete not partial redistribution of photons in the lines, which overestimates the Ca H & K line cooling and partially compensates for the neglect of the Mg II h & k lines (Uitenbroek 2002). There is no line blanketing. Finally, there is no magnetic field.

One prediction of the Carlsson & Stein (1995,2002) calculations is that in non-magnetic regions there is insufficient acoustic shock heating to raise the average chromospheric temperature below where absorption of coronal radiation in the helium continua begins to heat the chromosphere. There is possible disagreement with SUMER observations that the cores of the N I, O I, C I and C II lines formed in the mid and upper chromosphere show emission everywhere. Although these lines are formed below the height where coronal radiation heating raises the mean chromospheric temperature, there is some contribution from that region which causes the line cores to be in emission everywhere, although weaker than observed.

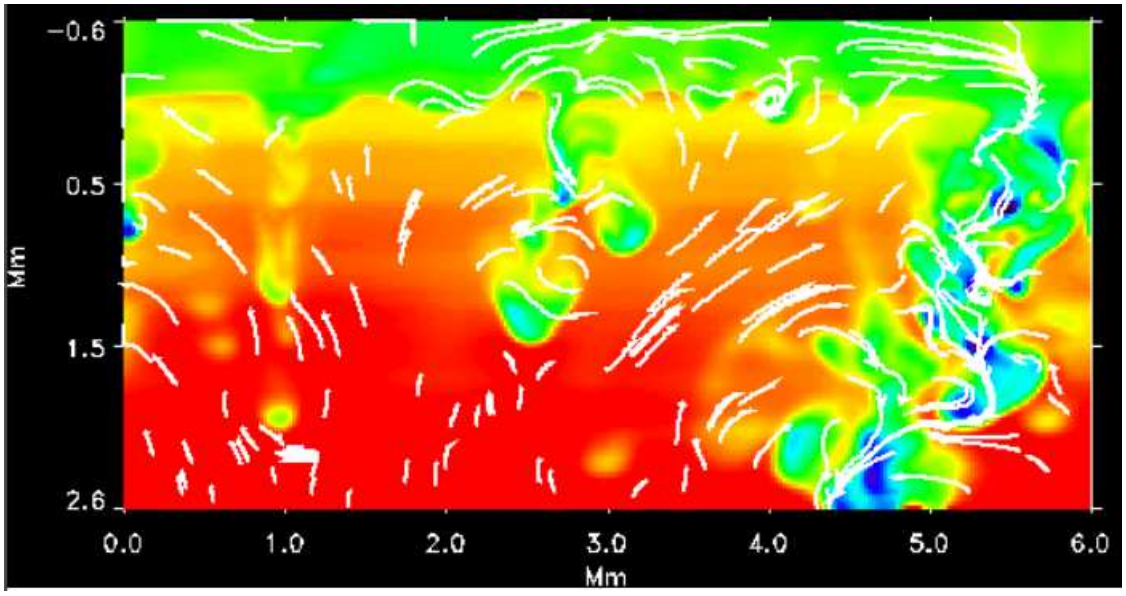

Figure 3. Temperature fluctuations and flow velocities on a vertical slice through the simulation domain. Red is hot and blue is cool. The fairly laminar upflows and turbulent downflows are clear.

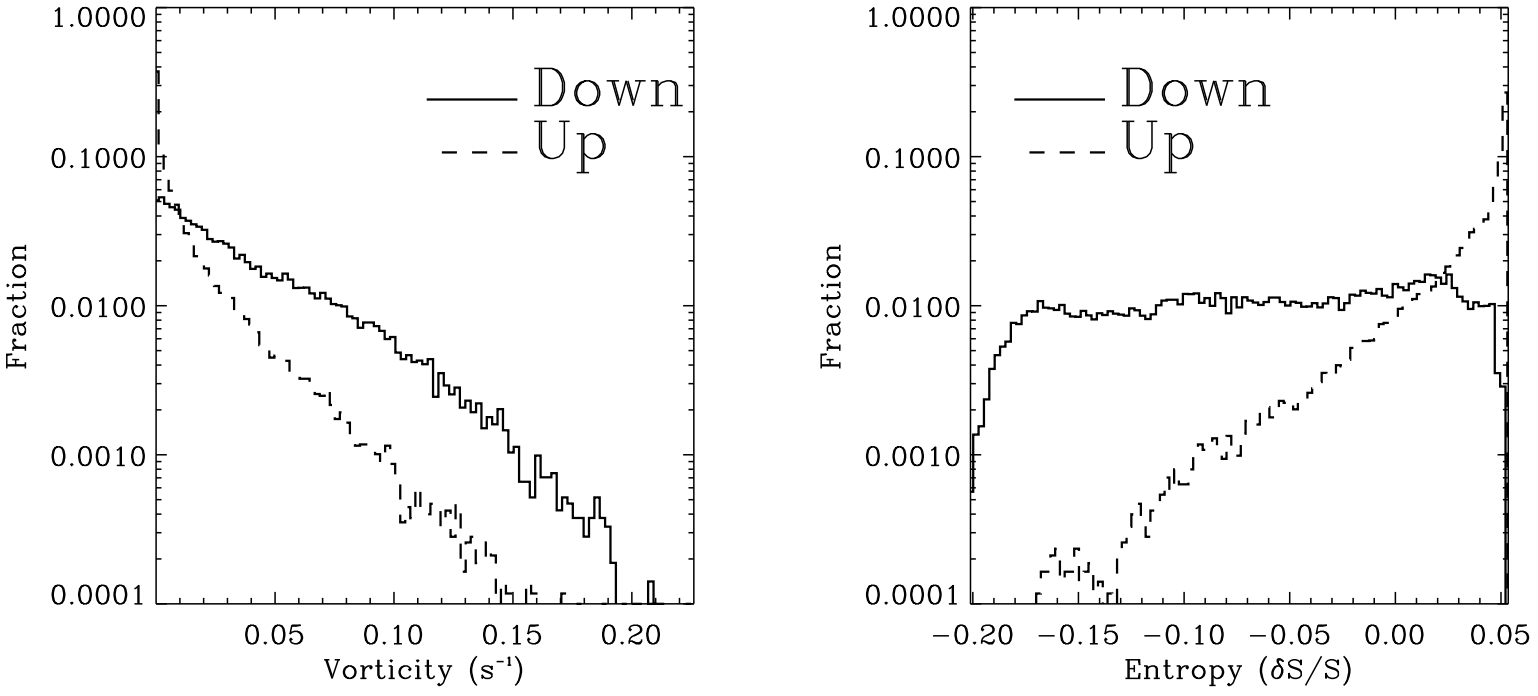

Figure 4. Vorticity (left) and entropy (right) probability distribution function separately for upflows and downflows near the surface.

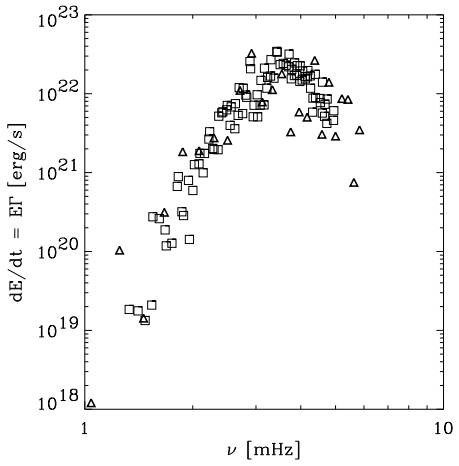

Figure 5. Comparison of observed and calculated p-mode excitation rates for the entire Sun. Squares are from SOHO golf observations for $\ell = 0 - 3$ (Roca Cortes 1999) and triangles are the simulation calculations.

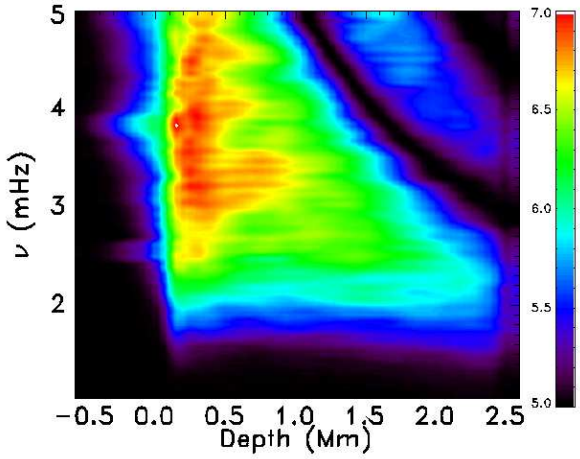

Figure 6. P-mode driving work as a function of frequency and depth. This is the integrand of eqn. 7.

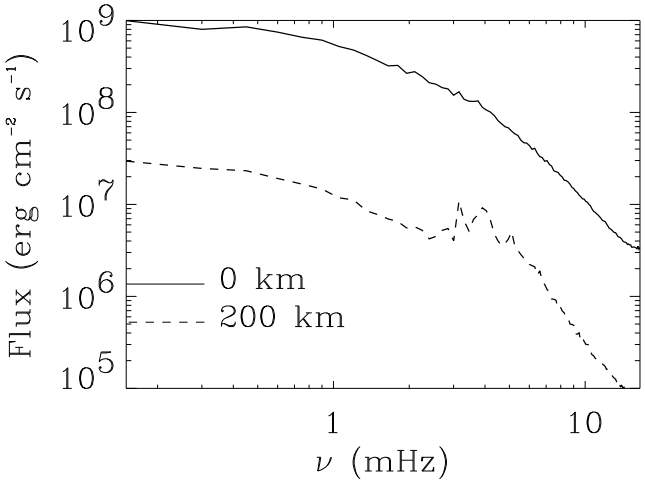

Figure 7. Acoustic flux at the visible surface and 200 km up in the photosphere.

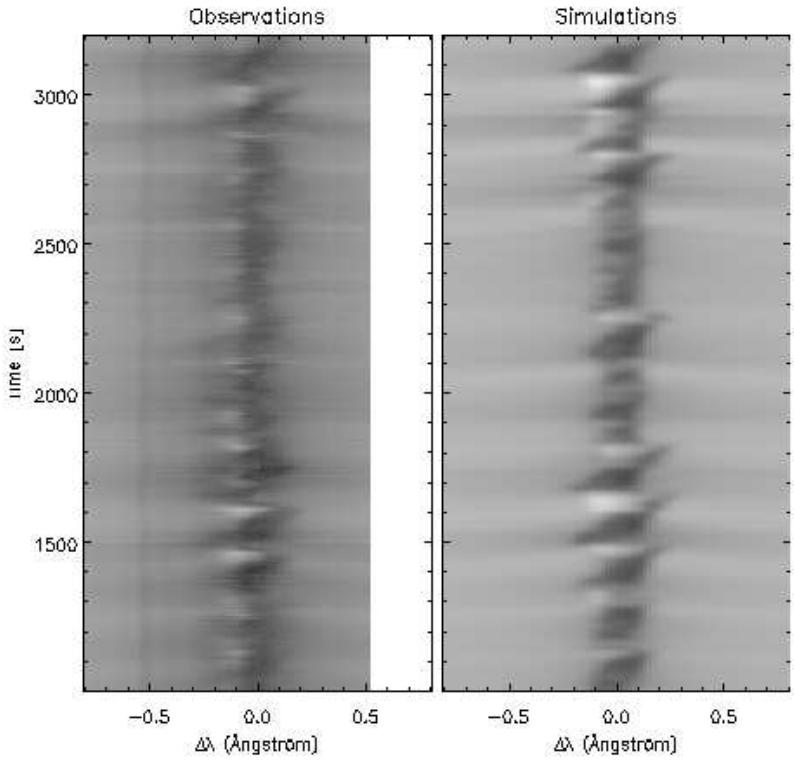

Figure 8. Observed and simulated Ca II H line intensities. The observed intensity fluctuations are closely reproduced by the simulations.

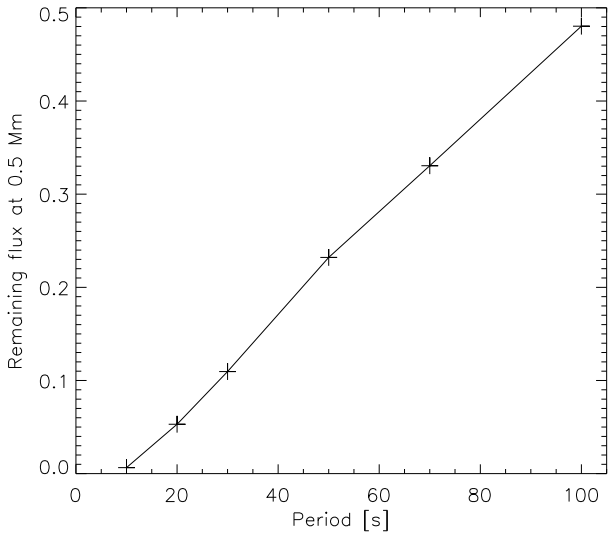

Figure 9. Fraction of acoustic flux reaching a given height above the visible surface as a function of wave frequency due to radiation damping.

Some have argued (Theurer, Ulmschneider & Cuntz 1997, Kalkofen, Ulmschneider & Avrett 1999) that there are unobservable higher frequency acoustic waves (30-50 mHz) in the Sun that produce extra shock heating. We view this as unlikely for two reasons – first, high resolution convection simulations (Stein & Nordlund 1998) with a grid size of 25 km horizontally and 15-35 km vertically should be able to easily resolve waves with wavelengths greater than 250 km or periods greater than 35 sec. These simulations show an acoustic flux spectrum decreasing with increasing frequency (Fig. 7), second, even if such high frequency waves were generated in the convection zone, they would be severely damped by radiation in the photosphere and be unable to transport significant energy to the chromosphere (Fig. 9). An obvious alternative candidate for extra heating is magnetic waves, since these simulations did not include a magnetic field. Magnetic fields will thread a significant fraction of the solar atmosphere by a height of 1 Mm.

It is difficult to observe waves in the chromosphere. The density is low so collisional transition rates are slow compared to dynamical time scales. There is not enough time to reach equilibrium. The radiation field is weak, since the chromosphere is illuminated only from below, so up/down radiative transitions do not balance (non-LTE). Ionization stages and molecular abundances do not have their equilibrium values. The source function is decoupled from the local temperature. The width of the line contribution functions is larger than the thickness of the shock structures and comparable to the wavelength of the waves. What we observe is an integral over an inhomogeneous region.

4. MAGNETO-HYDRODYNAMIC WAVE PROPAGATION

In the presence of a magnetic field many wave types (not just sound and internal gravity) exist – fast, slow and Alfvén waves, sausage, kink and torsional tube waves, and magneto-gravity waves. These MHD waves likely play a role in providing the extra heating observed above the magnetic network and in plages. They have been observed in chromosphere, coronal loops, the solar wind, and the interstellar medium. The coupling and interchange of energy among these various modes by both linear and non-linear processes has been extensively studied because of its importance in the transmission of energy to the chromosphere and corona and in the heating of these regions. Most analytic work has assumed a magnetic field either parallel or perpendicular to the stratification (but see Stein 1971).

The general case requires numerical simulations, and we have begun to study the coupling, transmission and reflection of mhd waves in a stratified atmosphere beginning with two simple cases, first magnetic field and plasma motions confined to only two dimensions and second vertically propagating fast waves driven from a weak field region with a complex field geometry. We find that the $\beta = P_{\rm gas}/P_{\rm magnetic} \approx 1$ surface likely represents what is referred to as the "magnetic canopy", not a surface defined by the spreading field lines filling up the entire area. It is the surface (at least in these two cases) where significant wave reflection and mode coupling occurs (Bogdan et al. 2003). This is illustrated for the case of vertical propagation in slanted structured field (Fig. 10), which shows the vertical velocity as a function of height and time. The top row shows the results for adiabatic waves. For a nearly vertical field there is little reflection and almost all the energy is transfered at the $\beta = 1$ surface, where the sound and Alfvén speeds are equal, from the incident acoustic fast wave to the transmitted acoustic slow wave, both traveling at the sound speed. For a highly tilted field there is significant reflection at the $\beta = 1$ surface and most of the transmitted energy is in the form of magnetic fast waves traveling at the Alfvén speed. When radiation losses are included (bottom row) the amplitude at the $\beta = 1$ surface is reduced which greatly reduces the wave reflection as well as the energy in the transmitted wave.

Next we look at what happens for localized wave driving in 2D (Bogdan et al. 2003). First consider the case of vertical driving in a stretch 0.5 Mm wide where $\beta > 1$ and the field is nearly vertical. This produces an acoustic fast wave in the weak field lower layers. Figure 11 shows the wave as it has just reached the $\beta = 1$ surface. The wave is visible in density, parallel and perpendicular velocities to the field, although the parallel velocity amplitude is greater than the perpendicular velocity amplitude. The wave is propagating spherically, but faster and with larger amplitude in the vertical direction because the propagation speed increases with height. No waves have yet been excited in the strong field region above $\beta = 1$. Figure (12)is for twice the time. The acoustic slow wave it shows up in the density fluctuations and velocity parallel the field has propagated almost half way from the $\beta = 1$ surface to the upper boundary. Ahead of it a magnetic fast wave with little density fluctuation and large perpendicular velocity amplitude has almost reached the upper boundary. This fast magnetic wave is generated at spreading locations on the $\beta = 1$ surface as the 2D propagating acoustic fast wave impinges on that layer. Note the break in the density and parallel velocity patterns just below the $\beta = 1$ surface due to interference with reflected acoustic fast waves.

Now consider the case of horizontal driving in the same configuration. This produces primarily a magnetic slow mode in the weak field layers. Figure (13) shows the wave just as the main front is just reaching the $\beta = 1$ surface. However, now it is the velocity perpendicular to the magnetic field that has the dominant amplitude, there are no visible density perturbation, and the wave is confined to the field lines that thread the piston, because this is primarily a magnetic slow wave. There is some indication in the perpendicular velocity of a much weaker wave front propagating spherically and already in the low β region. This is a weak acoustic wave that was also produced by the driving piston and arrived at the $\beta = 1$ surface earlier because the sound speed is larger than the Alfvén speed in the weak field layers. The next figure (14) is slightly later. Part of the magnetic slow mode first wave front has past through the $\beta = 1$ surface and is beginning to spread out beyond the driving field lines as a magnetic fast wave in the strong field upper layers. A slight bit

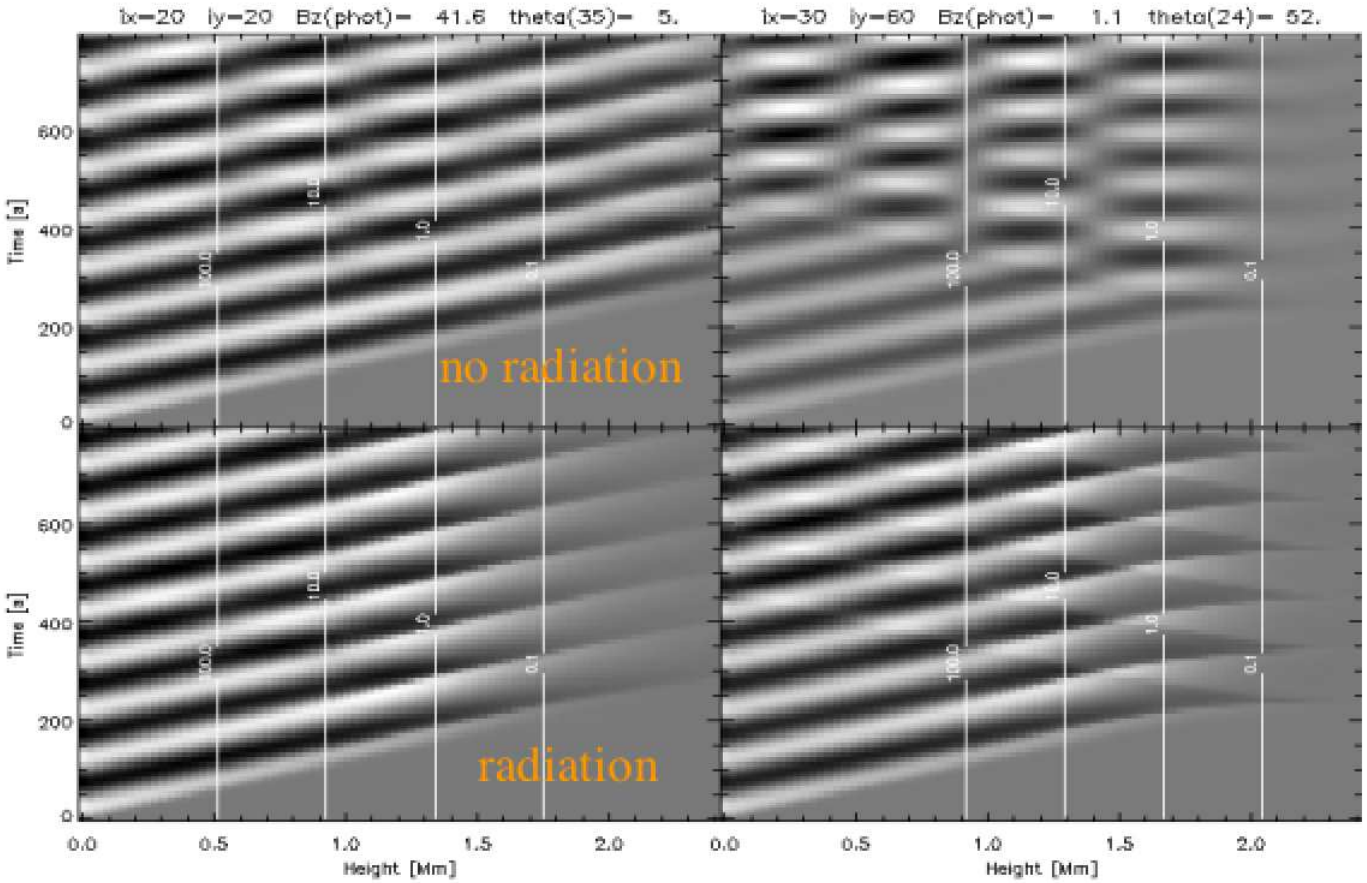

Figure 10. Vertically propagating waves in a nearly vertical field (5^o left) and a highly inclined field (52^o right)

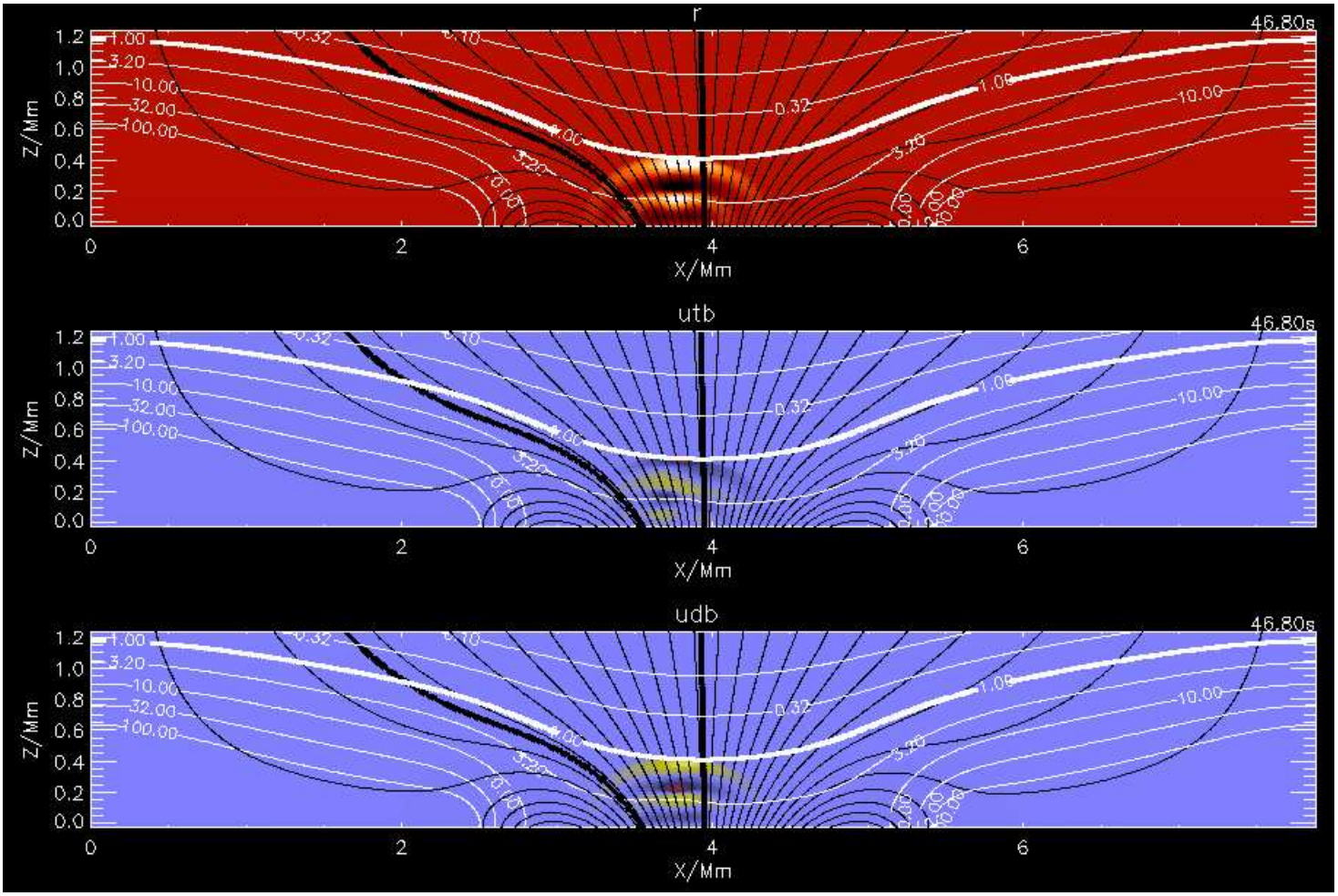

Figure 11. Vertically driven waves in a diverging 2D field geometry. The field is weak at the driving piston. $\beta = 1$ is shown by a thick white line. Individual field lines are shown in black. The top panel is the density, the middle panel the velocity perpendicular to the magnetic field and the bottom panel the velocity parallel the magnetic The driven acoustic fast wave has just reached the $\beta = 1$ surface. field.

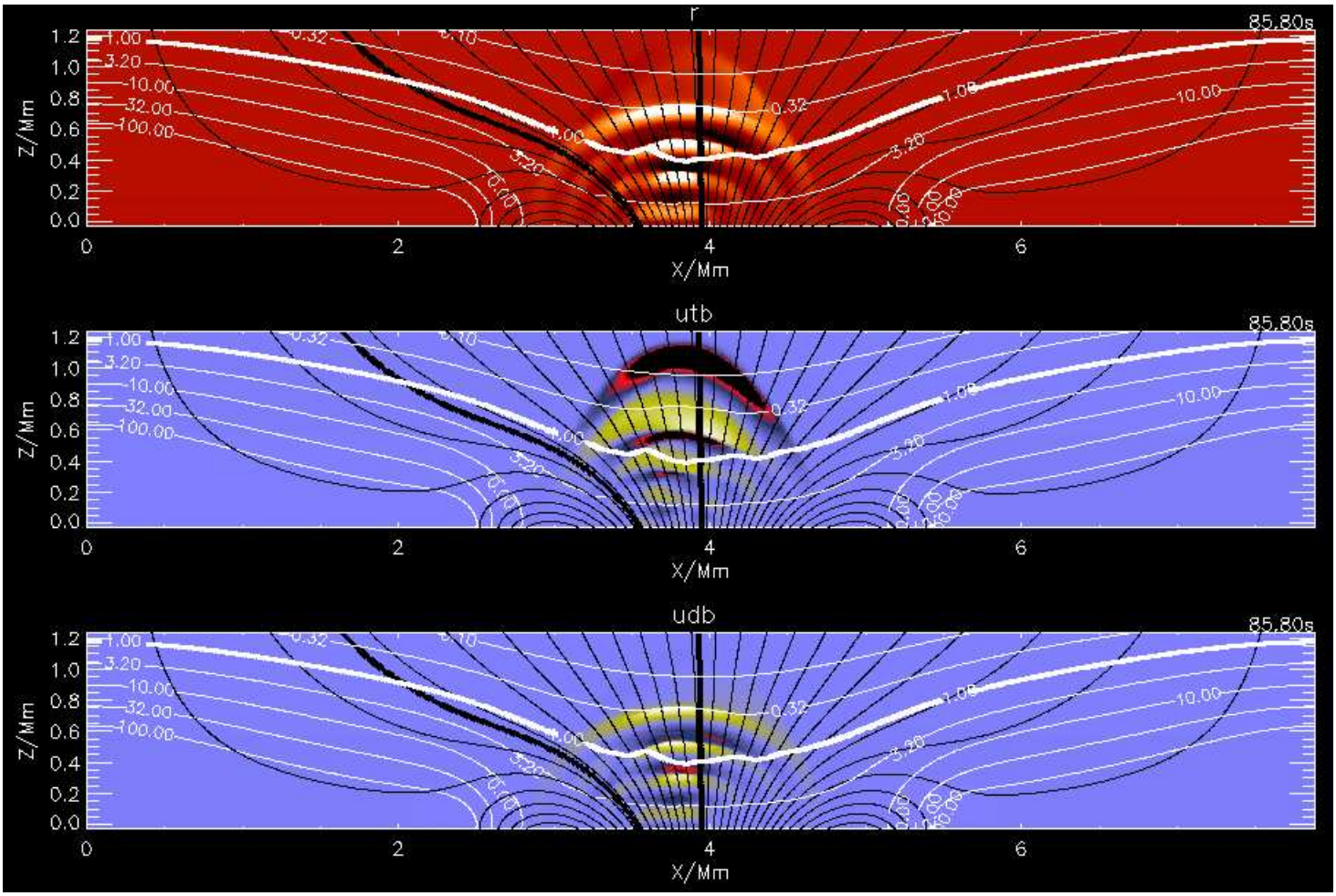

Figure 12. The same as Fig. 11 except later. The fast magnetic wave in the strong field layers has almost reached the top boundary.

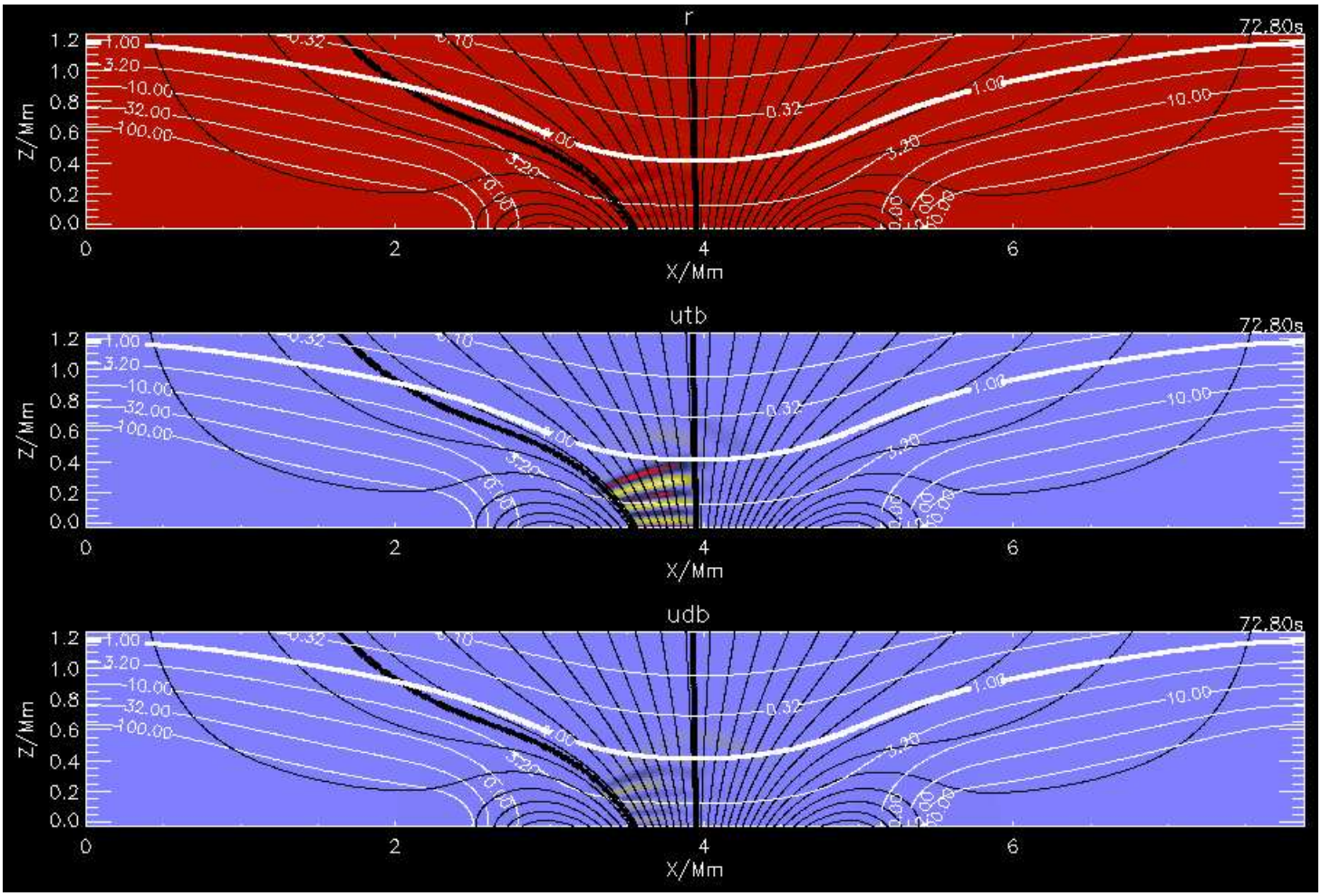

Figure 13. Horizontal driving case. This produces a slow magnetic wave in the weak field layers, which has just reached the $\beta = 1$ surface.

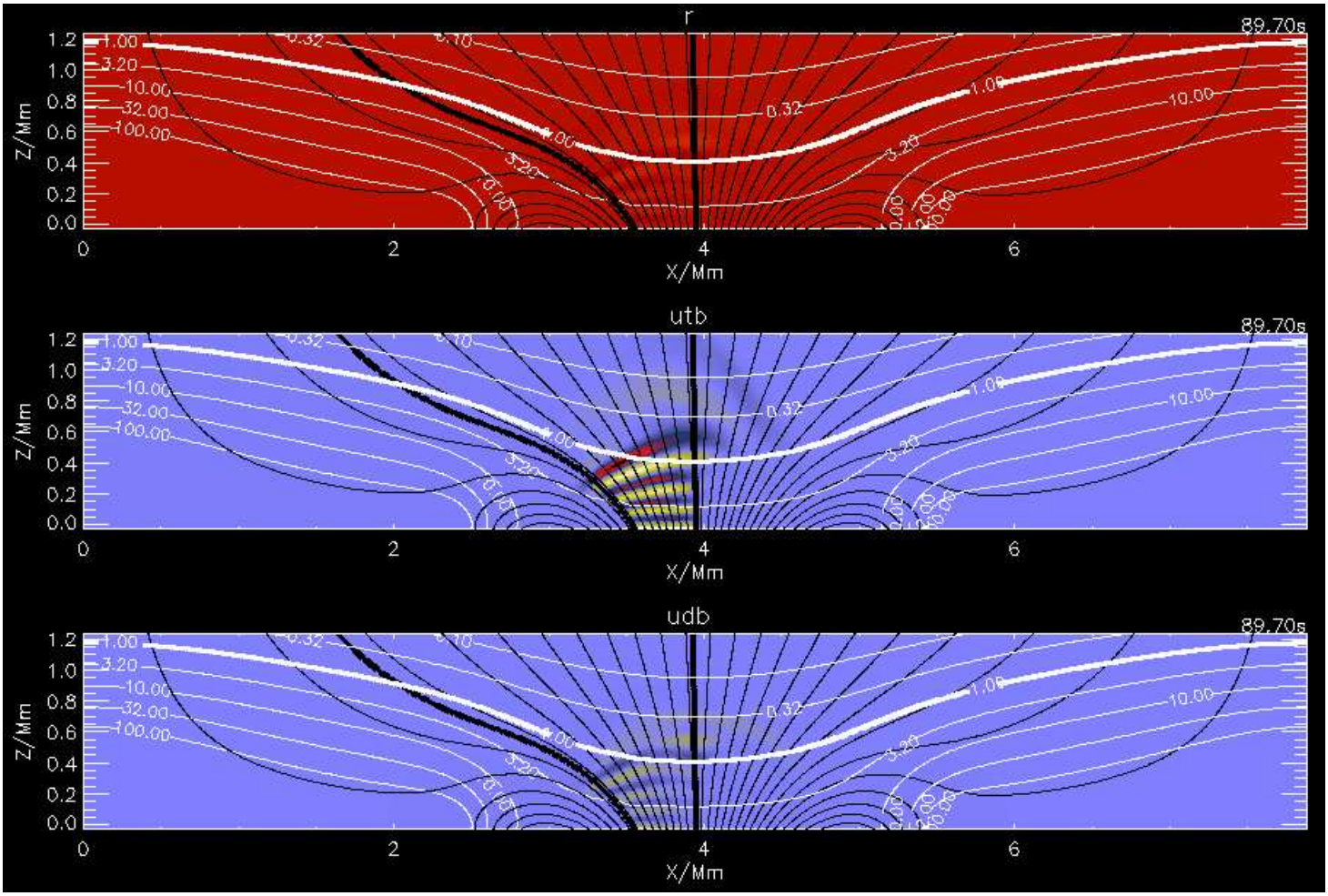

Figure 14. Horizontal driving case, slightly later. The slow magnetic wave has now past partly through the $\beta = 1$ surface and is beginning to spread out as a magnetic fast wave.

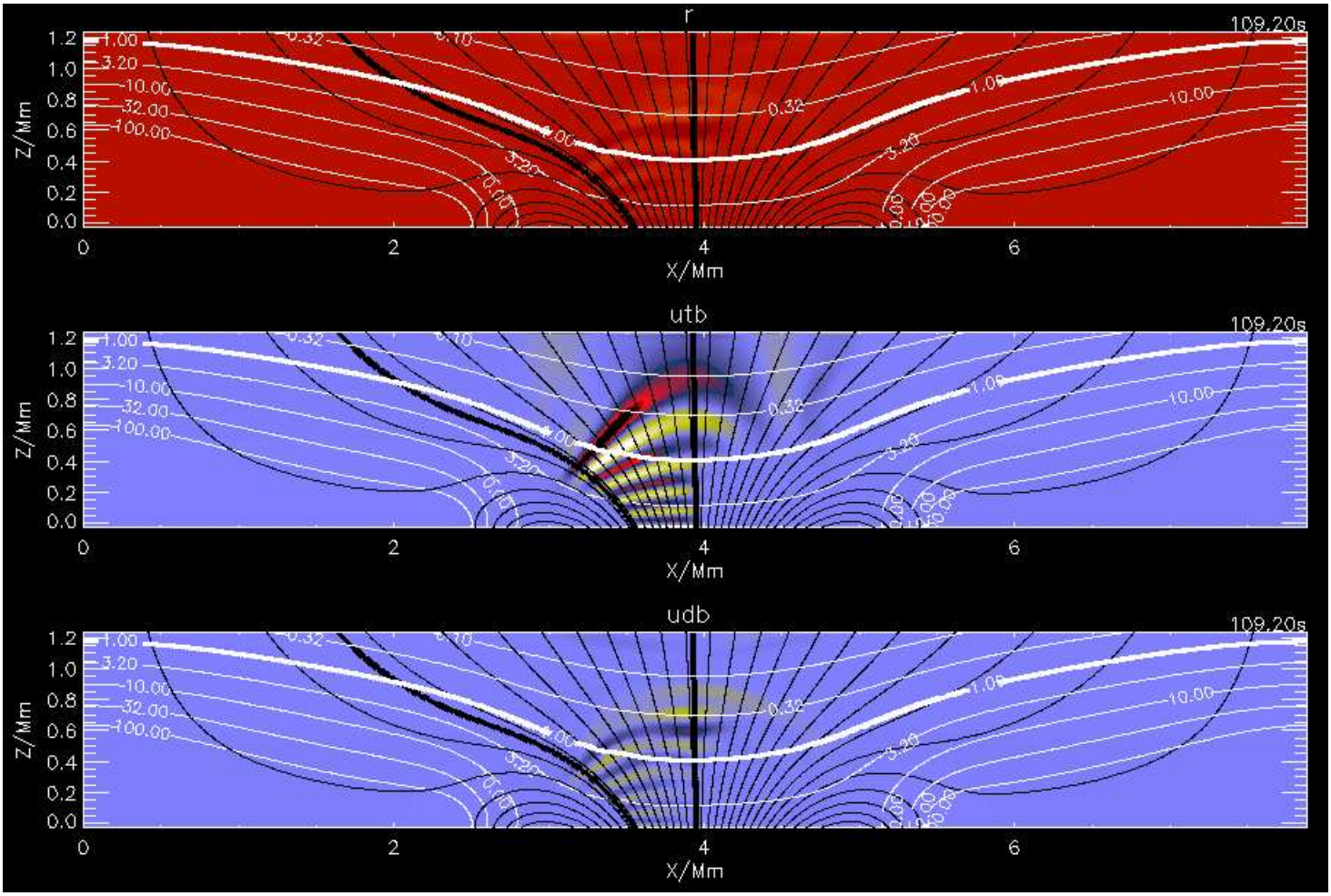

Figure 15. Horizontal driving case, still later. The primary magnetic wave has now almost reached the top boundary and the weak magnetic fast wave has now passed through the upper boundary and its wings are being refracted back down.

of density enhancement can now also be seen. The magnetic wave produced by the small amplitude acoustic fast wave hitting the $\beta = 1$ surface earlier is just reaching the upper boundary. Slightly later still, figure (15) shows the primary fast wave almost at the upper boundary. It is propagating much faster than before, as shown by the wider spacing between waves, also spreading out beyond the driving field lines. It has produced some density perturbations. The weak first fast wave that was excited has past through the upper boundary and its slower moving wings are being refracted back down as shown by the light nearly vertical fronts in the perpendicular velocity. For further details see Bogdan et al. (2003).

ACKNOWLEDGMENTS

This work was supported by NASA grants NAG 5-9563 and NAG 5-124350, and NSF grantAST 0205500. This support is greatly appreciated.

REFERENCES

Alfvén, H., 1947, MNRAS 107, 211

Arregui, I., Oliver, R., Ballester, J. L., 2003, A&A 402, 1129

Balmforth, N. J., 1992, MNRAS 255, 639

Bazer, J., 1961, N.Y.U. Res. Rpt. MH-11

Biermann, L., 1948, Zs. f. Astrophys. 25, 161

Bodo, G., Kalkofen, W., Massaglia, S. Rossi, P., 2000, A&A 354, 296

Bogdan, T. J., Carlsson, M., Hansteen, V., McMurry, A., Rosenthal, C. S., Johnson, M., Petty-Powell, S., Zita, E. J., Stein, R. F., McIntosh, S. W., Nordlund, Å., 2003, ApJ (in press)

Buchholz, B., Ulmschneider, P., Cuntz, M., 1998, ApJ 494, 700

Cally, P. S., 1986, Sol. Phys. 103, 277

Cargill, P. J., Spicer, D. S., Zalesak, S. T., 1997, ApJ 488, 854

Carlsson, M., Stein, R. F., 1992, ApJL 397, L59

Carlsson, M., Stein R. F., 1995, ApJL 440, L29

Carlsson, M., Stein R. F., 1997, ApJ 481, 500

Cuntz, M., Rammacher, W. Ulmschneider, P., Musielak, Z. E., Saar, S. H., 1999, ApJ 522, 1053

De Groof, A., Goossens, M., 2000, A&A 356, 724

De Groof, A., Paes, K., Goossens, M., 2002, A&A 386, 691

De Moortel, I., Hood, A. W., Arber, T. D., 2000, A&A 354, 334

Fawzy, D., Rammacher, W., Ulmschneider, P., Musielak, Z. E., Stepien, K., 2002, A&A 386, 971

Frisch, U., 1964, Ann. d'Ap. 27, 224

Goldreich, P., Murray, N., Kumar, P., 1994, ApJ 424, 466

Goodman, M. L., 2000, ApJ 533, 501

Goossens, M., De Groof, A., 2001, Phys. Plasmas 8, 2371

Heyvaerts, J., Prest, E. R., 1983, A&A 117, 220

Huang, P., Musielak, Z. E., Ulmschneider, P., 1999, A&A 342, 300

Ionson, J. A., 1978, ApJ 226, 650

Kalkofen, W., Ulmschneider, P., Averett, E. H., 1999, ApJL 521, 141L

Kulsrud, R. M., 1955, ApJ 121, 461

Lee, M. A., Roberts, B. 1986, ApJ 301, 430

Lighthill, M. J., 1952, Proc. Roy. Soc. London, A 211, 564

Lighthill, M. J., 1960, Phil. Trans. Roy. Soc. London A 252, 397

Luo, Q. Y., Wei, F. S., Feng, X. S., 2002, A&A 395, 669

Mckenzie, J. F., Axford, W. I., 2000, Sol. Phys. 193, 153

Musielak, Z. E., 1995, ApJ 452, 434

Musielak, Z. E., Rosner, R., Stein, R. F., Ulmschneider, P., 1994, ApJ 423, 474

Musielak, Z. E., Ulmschneider, P., 2001, A&A 370, 541

Musielak, Z. E., Ulmschneider, P., 2003, A&A 406, 725

Nordlund, Å., Stein, R. F., 2001, ApJ 546, 576

Osterbrock, D. E., 1961, ApJ 134, 347

Proudman, I., 1952, Proc. Roy. Soc. London, A 214, 119

Rammacher, W., Cuntz, M., 2003, ApJL 594, L51

Roca Cortes, T., Montanes, P., Palle, P. L., Perez Hernandez, F., Jimenez, A., Regula, C., the GOLF Team 1999, in A. Gimenez, E. Guinan, B. Montesinos (eds.), Theory and Tests of Convective Energy Transport, ASP Conf. Ser. 173, 305

Sakai, J. I., Minamizuka, R., Kawata, T. Cramer, N. F., 2001, ApJ 550, 1075

Samadi, R., Goupil, M.-J., 2001, A&A 370, 136

Skartlien, R., Stein, R. F., Nordlund, Å., 2000, ApJ 541, 468

Stein, R. F., 1967, Sol. Phys. 2, 385

Stein, R. F., 1971, ApJS 22, 419

Stein, R. F., Nordlund, Å., 1998, ApJ 499, 914

Stein, R. F., Nordlund, Å., 2000, Sol. Phys. 192, 91

Stein, R. F., Nordlund, Å., 2001, ApJ 546, 585

Stenuit, H., Keppens, R., Goossens, M., 1998, A&A 331, 392

Theurer, J., Ulmschneider, P., Cuntz, M., 1997, A&A 324, 587

Tirry, W. J., Berghmans, D. 1997, A&A 325, 329

Tsiklauri, D., Nakariakov, V. M., Rowlands, G. 2003, A&A 400, 1051

Uitenbroek, H., 2002, ApJ 565, 1312

Ulmschneider, P., Musielak, Z. E., 1998, A&A 338, 311

Unno, W., Kato, S., 1962, PASJ 14, 416

Ziegler, U., Ulmschneider, P. 1997, A&A 324, 417